Journal of Solid State Chemistry **145,** 327–335 (1999)
Article ID jssc.1999.8288, available online at http://www.idealibrary.com on IDEAL®

Vegard's Rule Revisited in $Ba_xPb_{1-x}(NO_3)_2$ by NMR and XRD[1]

Guy A. Crundwell,*,[2] Brett A. Cowans,† Jeffrey A. Hopkins,*,[3]
John B. Grutzner,* and Bart Kahr‡,[4]

*Department of Chemistry and †School of Chemical Engineering, Purdue University, West Lafayette, Indiana 47907; and
‡Department of Chemistry, Box 351700, University of Washington, Seattle, Washington 98195

Received November 9, 1998; accepted March 23, 1999

Vegard's rule, originally based on powder X-ray diffraction data from $Ba_xPb_{1-x}(NO_3)_2$, is reevaluated through the application of nuclear magnetic resonance (NMR) spectroscopy. Solid state ^{207}Pb NMR and ^{15}N NMR spectra of $Ba_xPb_{1-x}(NO_3)_2$ ($0.93 > x > 0.08$) were recorded. The chemical shift dispersions for each magnetic nucleus are remarkable for their sensitivity to the nearest neighbor Pb^{2+} and Ba^{2+} distributions. The intensities of the peaks in the ^{207}Pb spectra and their deviations from a simple binomial dependence reveal a non-statistical incorporation of Ba^{2+} and Pb^{2+} in the bulk crystals. Complementary analyses were performed by powder X-ray diffraction and with electron spectroscopy for chemical analysis that reveal bulk heterogeneities varying with crystal growth conditions. Vegard's original determination of a linear correlation between lattice constants and composition in Ba_xPb_{1-x} $(NO_3)_2$ is shown to have been a favorable consequence of the low resolution X-ray film methods available in the 1920s, but his additivity relationship is restored locally in the linear correlation of chemical shift with composition of the first metal coordination sphere.

INTRODUCTION

Mixed crystals of the isomorphous salts $Ba(NO_3)_2$ and $Pb(NO_3)_2$ served as the chemical system upon which Vegard established his *law* or *rule* (1), a long-standing empirical principle which recognizes that for some miscible solids the lattice constant varies linearly with composition (Fig. 1) (2). Chemists have paid a great deal of attention to how and why mixed crystal systems violate Vegard's rule (VR) (3). We show that even the foundational systems which established and obey this rule display a great deal of chemistry and rich textures otherwise masked by the tidy additivity relationship provided by Vegard.

We were first attracted to $Ba_xPb_{1-x}(NO_3)_2$, because, despite its adherence to VR, it is among the prototypical so-called optically anomalous crystals that have optical symmetries incompatible with their morphological symmetries (4). Such anomalies were typically disregarded by the early pioneers of X ray crystallography such as Vegard. We recently presented an X-ray study of $Ba_xPb_{1-x}(NO_3)_2$ single crystals that are morphologically cubic yet optically anisotropic (5). We found that nonstatistical occupation of cation sites, as well as an obverse/reverse twinning of the unit cell could be implicated as causes for the anomalous birefringence. Nevertheless, a quantitative correlation between the birefringence of the mixed crystals with their X-ray structure was not forthcoming. Here we complement that earlier work, by studying Ba_xPb_{1-x} $(NO_3)_2$ with solid state NMR spectroscopy, an atomic scale probe of crystalline fine structure (6, 7).

EXPERIMENTAL

Synthesis and Crystal Growth

Mixed crystals of $Ba_xPb_{1-x}(NO_3)_2$ were grown by slow evaporation of aqueous solutions of $Ba(NO_3)_2$ and $Pb(NO_3)_2$ (Aldrich, 99.98% and 99.99%, respectively) at room temperature ($22^\circ C \pm 2^\circ$) or by the slow crystallization of up to 2 L solutions in dishes submerged in a water bath at $25.0^\circ C$ ($\pm 0.1^\circ$).

The ^{15}N enriched salts were precipitated from $Na^{15}NO_3$ (^{15}N, 98+%, Cambridge Isotopes), and $BaCl_2$ (Baker, 99.7%) or $PbSiF_6 \cdot 2H_2O$ (Pfaltz and Bauer). The formation of $Pb(^{15}NO_3)_2$ was verified by both ^{207}Pb and ^{15}N MAS NMR.

[1]Based on the Ph.D. dissertation of G. Crundwell, Purdue University, 1996. During the preparation of this manuscript we have become aware of a similar study on the ^{207}Pb NMR spectra of solid solutions of divalent metal nitrates, especially Sr^{2+} (see Y.-S. Kye and G. S. Harbison, *Inorg. Chem.* **37,** 6030 (1998).

[2]Present address: Department of Chemistry, Central Connecticut State University, New Britian, CT 06050.

[3]Present address: General Electric Company, P.O. Box 414, W-832, Milwaukee, WI 53021.

[4]To whom correspondence should be addressed. E-mail: kahr@chem.washington.edu.

0022-4596/99 $30.00

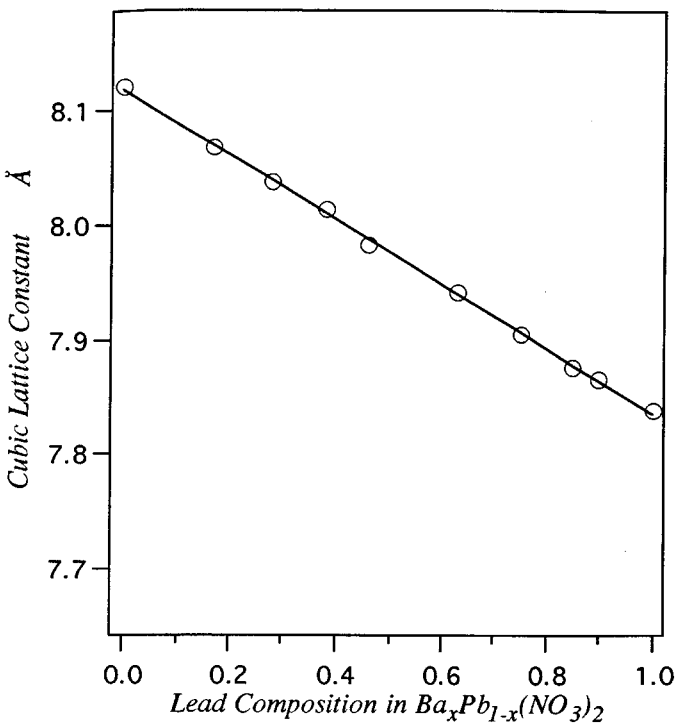

FIG. 1. Data from Ref. (1) showing the original formulation of Vegard's rule.

Homogeneous powders of Pb^{2+}, Ba^{2+}, Sr^{2+}, and Ca^{2+} nitrates were precipitated by the addition of concentrated HNO_3 to saturated solutions, according to the procedure of Rao and co-workers (8). Upon precipitation, the powders were filtered and allowed to dry in a dessicator since mixed powders containing $Ca(NO_3)_2$ deliquesce slowly when exposed to air.

Optical Crystallography

Optical properties of mixed crystals were studied with an Olympus BH-2 polarizing microscope in orthoscopic and conoscopic illumination. Thin sections for optical crystallography were mounted in epoxy, cut using a diamond saw, and protected by cover glasses. The retardation was measured with a Berek compensator.

Solid State NMR

^{207}Pb and ^{15}N MAS NMR spectra were acquired on a GE-Omega 400WB spectrometer operating at 83.41 MHz for ^{207}Pb and 40.56 MHz for ^{15}N. Samples were ground in a mortar and packed into a 5-mm zirconia rotor (Doty). Samples were spun at rates ranging between 1–4 kHz in a Doty Scientific HS-MAS probe. Chemical shift anisotropy (CSA) patterns were obtained on static samples and with slow (1–2 kHz) spinning. Data was acquired in single pulse mode (without proton decoupling). For the experiments involving ^{207}Pb, the FIDs (collected as 4 K complex points) were usually 33 K scans (unless fewer scans gave reasonable signal to noise) that were acquired with a pulse width of 3 μs, a spectral width of 200 kHz, an acquisition time of 20.5 ms, and a recycle delay of 2 s. All ^{207}Pb spectra were externally referenced to pure $Pb(NO_3)_2$ in solution set at 0 ppm ($\delta = -3474$ ppm relative to $Pb(CH_3)_4$). For the experiments involving ^{15}N, the FIDs (collected as 2 K complex points) of 64 scans were acquired with a pulse width of 4 μs, a spectral width of 20 kHz, an acquisition time of 51.2 ms, and a recycle delay of 60 s. ^{15}N spectra were referenced to ^{15}N enriched solid glycine set to 0 ppm. All spectra were taken at ambient temperature, 20°C ($\pm 1°$). Computer simulations of the ^{207}Pb MAS anisotropic spinning sideband patterns for $Ba_xPb_{1-x}(NO_3)_2$ crystals were performed on a Sun workstation using the program MASCSA (9).

Electron Microprobe Analysis

Crystals were cut and polished prior to being mounted in epoxy for microprobe analysis. The epoxy slugs were gently polished and covered with a carbon film to dissipate the static charge. The spectroscopy was carried out on a CAMECA SX-50 electron microprobe operating at 15 kV, 20 nA, 30 s each element, with a 1-μm beam using CAMECA's PAP correction scheme. In some cases backscattered electron micrographs were made by scanning large $\sim$2 mm regions of the crystals. In these cases the current of the beam was varied to give maximum resolution between Pb-rich and Pb-poor regions of the crystals.

Powder X-Ray Diffraction

Individual mixed crystals were ground into powders that were then filtered through a mesh. Data were collected with a Scintag Incorporated XDS 2000 powder diffractometer running at 30 kV and 30 mA using Cu$K\alpha$ radiation ($\lambda = 1.5405$ Å). Spectra were recorded from $10° < 2\theta < 70°$. The data was corrected for $K\alpha_2$ radiation.

Atomic Absorption

The concentration of Pb was determined with a Perkin–Elmer Model 3110 Atomic Absorption Spectrometer. Samples were dissolved in 250 mL of distilled water targeted to give $[Pb^{2+}]$ between 0.5–4.0 mg L^{-1}. Standards were prepared over a similar Pb concentration range.

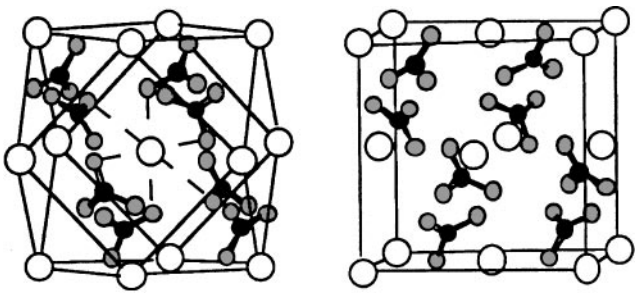

FIG. 2. The first coordination sphere (left) and the unit cell of $M(NO_3)_2$, where M = Ba, Pb (right). The open, filled, and half-filled atoms are M, N, and O atoms, respectively.

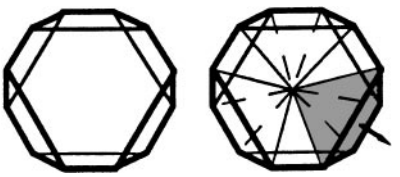

FIG. 4. The {1 1 1} morphology of $Ba(NO_3)_2$, $Pb(NO_3)_2$, and $Ba_xPb_{1-x}(NO_3)_2$ is shown on the left. The diagram on the right shows how the eight individual growth sectors tile to form an optically anomalous mixed crystal.

RESULTS AND DISCUSSION

Structure

$Ba(NO_3)_2$ and $Pb(NO_3)_2$ are isomorphous and crystallize in the space group, $Pa\bar{3}$, Z = 4, with the metal ions on S_6 sites (10, 11). They and their mixed crystals can be represented by a face-centered cubic array in which each cation has 12 cation neighbors at the vertices of a cubeoctahedron. These neighbors comprise two sets of six symmetry-related ions adopting axial and equatorial positions with respect to the central ion (Fig. 2). In a given unit cell, four Pb^{2+} ions are arranged at the vertices of a regular tetrahedron. Eight NO_3^- groups lie on the threefold axes and are planar but not crystallographically so with three nearest cations (d_{Ba-N} = 3.3240(3) Å, d_{Pb-N} = 3.2150(3) Å) that make unequal distances to nearest oxygen atoms (d_{Ba-O} = 2.7482(6) Å; 2.8688(6) and d_{Pb-O} = 2.8789(6) Å; 2.9414(6)). The nitrate group geometries are indistinguishable within experimental error ($d_{N-O(Ba)}$ = 1.2465(6); $d_{N-O(Pb)}$ = 1.2465(6)). The coordination shell of each Pb^{2+} contains six proximal nitrates arranged octahedrally. Two uncoordinated distal nitrates lie on that Pb^{2+} ion's threefold axis. When the oxygen layers are viewed perpendicular to the principal diagonal, the 24 unique oxygen atoms are arranged in layers of 3, 6, 6, 6, and 3 (see layers a–e in Fig. 3). The plane of the three oxygens perpendicular to the principal diagonal define the left and right (layers a, e); two sets of six oxygens are slightly twisted from coplanarity (layers b, d), half of which are coordinating the Pb^{2+} on the specified threefold axis, as is a set of six coordinating equatorial oxygens.

Inhomogeneous Crystals

Mixed crystals of $Ba(NO_3)_2$ and $Pb(NO_3)_2$ were grown by the original method of Vegard (1), by slow evaporation of aqueous solutions (< 500 mL) at room temperature

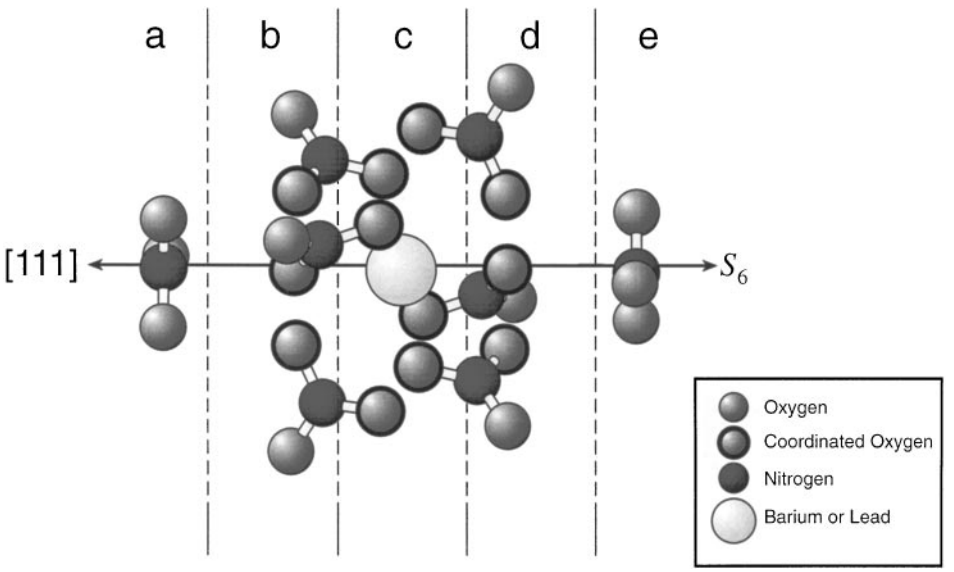

FIG. 3. The NO_3^- environment around a given M ion in $M(NO_3)_2$, where M = Ba, Pb.

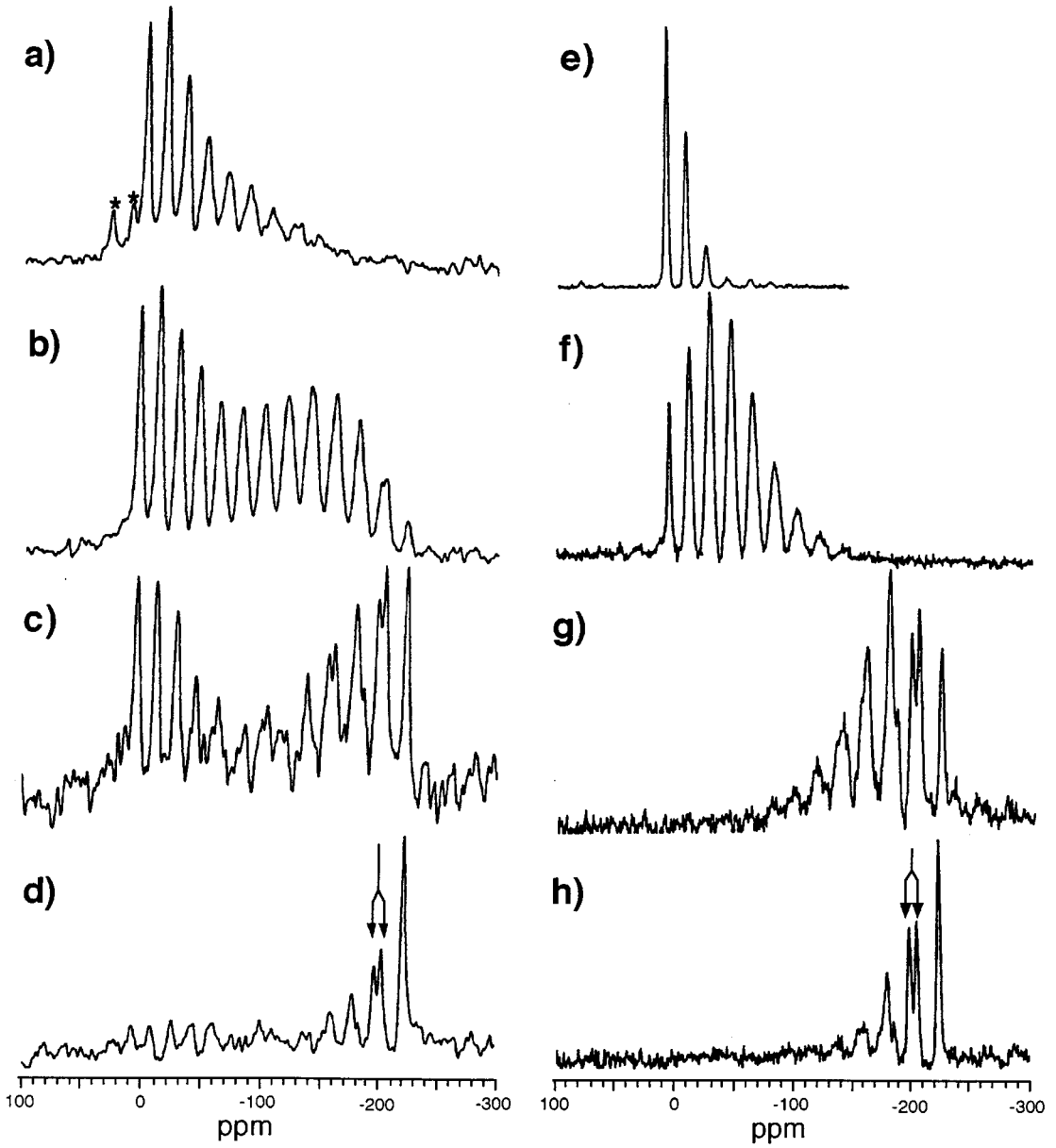

FIG. 5. ^{207}Pb MAS NMR powder spectra of ground single crystals grown by slow evaporation without (a–d) and with (e–h) an additional source of Pb^{2+} cations to compensate for the solubility difference between $Ba(NO_3)_2$ and $Pb(NO_3)_2$. The concentration of the crystals were: (a) $Ba_{0.35}Pb_{0.65}(NO_3)_2$; (b) $Ba_{0.54}Pb_{0.46}(NO_3)_2$; (c) $Ba_{0.75}Pb_{0.25}(NO_3)_2$; (d) $Ba_{0.93}Pb_{0.07}(NO_3)_2$; (e) $Ba_{0.06}Pb_{0.94}(NO_3)_2$; (f) $Ba_{0.31}Pb_{0.69}(NO_3)_2$; (g) $Ba_{0.72}Pb_{0.28}(NO_3)_2$; (h) $Ba_{0.89}Pb_{0.11}(NO_3)_2$. * marks spinning sidebands.

($22 \pm 2^{\circ}$). Alternatively, the dishes were maintained in water baths at $25.0 \pm 0.1^{\circ}$C, although this additional control seemed to have little effect on the subsequent analyses. The first crystals deposited were harvested. Inspection in crossed polarized light revealed that the crystals with a $\{1\,1\,1\}$ habit are composed of eight uniaxial growth sectors that are related to one another by the tetrahedral point symmetry (T_h) of the parent group $Pa\bar{3}$ (Fig. 4).

The solid state ^{207}Pb NMR spectrum of powdered $Pb(NO_3)_2$ was first published in 1958 (12). In 1977, Nolle reported the axially symmetric chemical shift anisotropy (CSA) as 56 ppm and the directions of its principal components in the unit cell (13). The ^{207}Pb MAS NMR spectrum of powdered $Pb(NO_3)_2$ shows a sharp singlet while the corresponding spectra of mixed crystals of $Ba_xPb_{1-x}(NO_3)_2$ that had been powdered with a mortar and pestle

show, to a first approximation, 13 equally spaced peaks (Fig. 5b). The position of the first peak very nearly corresponds to that of pure $Pb(NO_3)_2$. The subsequent upfield peaks can be conveniently assigned to local Pb^{2+} environments in which ions in the first coordination sphere are successively replaced by n Ba^{2+} ions ($n = 0, 1, 2, 3, \ldots, 12$). The separation between adjacent peaks is consistently 19.5(2) ppm. Fechtelkord and Bismayer recently used shifts induced by Ba-doping to distinguish Pb environments in ferroplastic $Pb_3(PO_4)_2$ crystals (6).

The relaxation times for each of the 13 peaks were recorded by the inversion recovery method. The 13 peaks all have relaxation times between 8–13 s. Thus, peak areas can reflect populations in a quantitative way so long as a sufficient relaxation time is chosen. Upon warming the sample from 20 to 40°C, all 13 peaks moved downfield with increasing temperature by 0.70 ppm/deg.

The intensity distributions in the ^{207}Pb spectra give valuable information on the mixed crystal growth. Ideally if the mixed crystals had incorporated guest cations statistically during growth, the intensities should follow the binomial distribution. However, it is quickly apparent from Figs. 5a–d, especially 5c, that the intensity distributions deviate considerably from the binomial distribution. Low-field and high-field portions of the spectra assigned to Pb^{2+} rich and Ba^{2+} rich local environments are considerably more intense than the intermediate admixtures. Backscattered electron micrographs and quantitative electron microprobe analysis showed clearly that the crystal heterogeneities were macroscopic. The heterogeneities arise logically from the solubility differences between $Ba(NO_3)_2$ and $Pb(NO_3)_2$ (87 gL^{-1} and 375 gL^{-1}, respectively) (14). The heterogeneities can be reduced, but not obviated, by harvesting the first crystals from increasingly large reservoirs ($\sim$2 L) so that the solution composition changes by $<5\%$.

Each peak in a ^{207}Pb spectrum has been assigned to distinct Pb^{2+}/Ba^{2+} ratios in the first coordination sphere. However, even ignoring the second coordination sphere, there may be multiple constitutional isomers for the first coordination sphere. The number of possible isomers can be determined by the application of Pólya's isomer enumeration theorem (15) in which elements of group theory and combinatorics are used to derive a polynomial whose coefficients correspond to the number of different constitutional isomers for a successively substituted frame. For the O_h cubeoctahedron Pólya's polynomial is

$$Z(FCC\text{-}O_h) = 1 + 1x + 4x^2 + 9x^3 + 18x^4 + 24x^5 + 30x^6 + 24x^7 + 18x^8 + 9x^9 + 4x^{10} + 1x^{11} + 1x^{12}. \quad [1]$$

Here, the orders of the polynomial terms correspond, for example, to the number of Ba^{2+} ions in the first coordination sphere while the coefficients refer to the number of constitutional isomers. Therefore, for Pb^{2+} surrounded by an ideal O_h cubeoctahedron of M^{2+} ions there is only one possible arrangement with 0, 1, 11, or 12 like-cations in the first coordination sphere. However, as shown above, there are four possible isomers when 2 or 10 Ba^{2+} ions occupy the cubeoctahedral framework and 30 isomers when six Ba^{2+} ions occupy the frame. Each isomer has a different energy and a unique $^{207}Pb^{2+}$ chemical shift, but obviously these distinctions have not been resolved in the spectra in Fig. 5.

In actual fact, we are dealing with a distorted cubeoctahedron with S_6 symmetry, the site symmetry of the metal ions in $Ba(NO_3)_2$ or $Pb(NO_3)_2$. The corresponding Pólya polynomial is given by formula (2) below. Here, we read that a single substitution produces two independent sets of six symmetry-related metal ions. This symmetry lowering upon substituting a single metal ion in the unit is routinely observed as a splitting (6 ppm) of the second most upfield peak that corresponds to a Pb^{2+} surrounded by one other Pb^{2+} and 11 Ba^{2+} ions:

$$Z(FCC\text{-}S_6) = 1 + 2x + 12x^2 + 38x^3 + 85x^4 + 132x^5 + 160x^6 + 132x^7 + 85x^8 + 38x^9 + 12x^{10} + 2x^{11} + 1x^{12}. \quad [2]$$

In static spectra the CSA for Pb^{+2} surrounded by 12 Ba^{+2} ions has the opposite sense and approximately half the magnitude of the CSA for Pb^{+2} surrounded by 12 lead ions. Substitution of a single Sr^{+2} in the nearest neighbor shell around lead, also reversed the sense of the CSA, but now the magnitude has doubled.

$Ba(^{15}NO_3)_2$ and $Pb(^{15}NO_3)_2$ were prepared from $Na^{15}NO_3$. The ^{15}N MAS NMR spectrum for pure

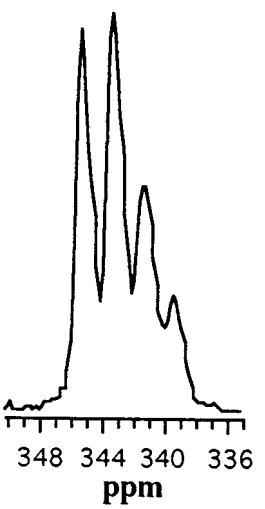

FIG. 6. The ^{15}N MAS NMR spectrum of $Ba_{0.59}Pb_{0.41}(^{15}NO_3)_2$.

$Pb(^{15}NO_3)_2$ shows a singlet at 340 ppm, whereas the ^{15}N MAS NMR spectrum for $Ba_{0.59}Pb_{0.41}(^{15}NO_3)_2$ is shown in Fig. 6. The four peaks (with a separation of 2 ppm) likely arise from the four combinations of three Pb^{2+} and/or Ba^{2+} ions surrounding a given NO_3^- group. This time, the successive replacement of Pb^{2+} by Ba^{2+} results in a downfield shift from the peak for $Pb(^{15}NO_3)_2$. Unlike the $^{207}Pb^{2+}$ spectra, the peaks in the ^{15}N spectrum have radically different relaxation times, making intensity comparisons difficult. An ^{15}N inversion recovery experiment was performed on $Ba_{0.59}Pb_{0.41}(^{15}NO_3)_2$ and the peak at 346 ppm (corresponding to the Ba^{2+}-rich environment) had a T_1 of about 10 min. The same inversion recovery experiment on a Pb^{2+}-rich $^{15}NO^{3-}$ ion gave a T_1 greater than 30 min.

Harbison and co-workers demonstrated that the principal elements of the ^{14}N quadrupole coupling constant and shielding tensor were colinear and were oriented along the body diagonals of the cubic unit cell, just like the Pb^{2+} shift (16). For both $Ba(NO_3)_2$ and $Pb(NO_3)_2$, the parallel (216 ppm) and perpendicular (438 ppm) components of the nitrogen chemical shift tensor were equal within experimental error. However, the quadrupole coupling constants differed by 20%, despite the identity of the nitrate dimensions determined by neutron diffraction. They concluded that the lattice packing is perturbing the charge distribution at nitrogen. Moore and co-workers determined ^{15}N shielding of NO_3^- ions in a series of salts theoretically and experimentally (17). They observed that N–O bond length variation from 1.23 Å (Na^+) to 1.27 Å (Ba^{2+}) increased the isotropic shift from -3.4 to 10 ppm. However, this model is based upon inaccurate bond length data. The N–O bond lengths in a variety of nitrate salts determined from neutron diffraction are constant within experimental error: Na^+, 1.248(1) Å (18); Sr^{2+}, 1.2467(5) Å (10); Pb^{2+}, 1.2465(6) Å (11); and Ba^{2+}, 1.2469(6) Å (10).

We have repeated Vegard's analysis of $Ba_xPb_{1-x}(NO_3)_2$ (1) using a modern powder diffractometer with an electronic detector. Unlike the end members, the mixed crystals show severe broadening and peak splitting at higher diffraction angles (Fig. 7). These data cannot be credibly fitted to a single cell. However, d values taken from the 2θ median of each broad cluster of peaks gave "cubic" unit cell lengths that nicely obey VR.

An electron microprobe was used to analyze Pb^{2+} and Ba^{2+} concentrations within individuals sectors of $\{1\,1\,1\}$ $Ba_xPb_{1-x}(NO_3)_2$ crystals. The beam traversed thin sections of exposed lateral sectors from the point of crystal nucleation to the edge of the crystal. In general it was seen that the incorporation of lead into the bulk was inhomogeneous. The first-grown sections of the sectors were depleted in lead. The negative of a backscattered electron micrograph of a crystal in cross section is shown in Fig. 8. The darker regions indicate increased backscatter near the crystal surface rich in Pb^{2+}. The center of the crystal contains only 10% lead, whereas the outermost regions contain as much as 70%. To further complicate matters, Tsuchiyama *et al.* have shown that the distribution coefficient can even vary from sector to sector within a single crystal and that it generally increases as growth rate increases (19). Vegard

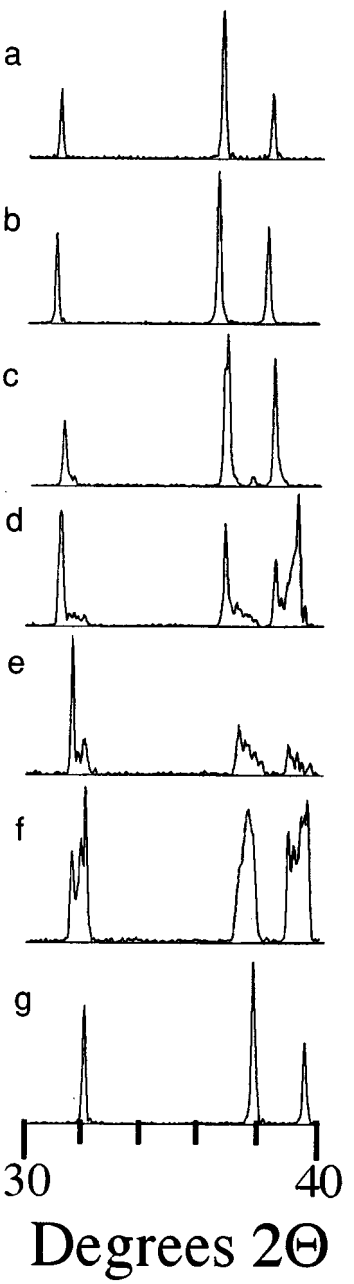

FIG. 7. X-ray powder diffraction spectra from $30 < 2\theta < 40°$ of mixed crystals of $Ba_xPb_{1-x}(NO_3)_2$ grown by the slow evaporation of solutions. The compositions of the crystals were: (a) $Ba(NO_3)_2$; (b) $Ba_{0.96}Pb_{0.04}(NO_3)_2$ Å; (c) $Ba_{0.87}Pb_{0.13}(NO_3)_2$; (d) $Ba_{0.65}Pb_{0.35}(NO_3)_2$; (e) $Ba_{0.54}Pb_{0.46}(NO_3)_2$; (f) $Ba_{0.35}Pb_{0.65}(NO_3)_2$; (g) $Pb(NO_3)_2$.

reported determining the concentration of his crystals with "great care" (grosse Sorgfalt) electrolytically, but he did not comment on nor account for the inhomogeneities (1).

Homogeneous Crystals

To compensate for the solubility difference between $Ba(NO_3)_2$ and $Pb(NO_3)_2$ mixed crystals of $Ba_xPb_{1-x}(NO_3)_2$ ($0.89 < x < 0.06$) were grown by adding 1.5 moles of $Pb(ClO_4)_2$ per mole of $Pb(NO_3)_2$ during the crystallization. The resulting spectra from ground samples of these mixed crystals are shown in Figs. 5e–h. Now the intensities nearly follow the expected binomial distribution. Microprobe analysis confirmed the bulk homogeneity. Crystals grown under both conditions are birefringent. There are no systematic correlations between the optical properties and compositional heterogeneity, which indicates that the composition does not have a simple relationship to the anomalous birefringence.

An alternative way to prepare homogeneous precipitates was described by Rao and co-workers (8) and applied to the series of isomorphous divalent nitrates $M(NO_3)_2$ (M = Ba, Sr, and Ca, Pb). In this procedure, aqueous solutions of nitrates were added to concentrated HNO_3, resulting in rapid reprecipitation. The ^{207}Pb MAS NMR spectra of the solids are shown in Fig. 9. The average spacing between the peaks is greatest for $Pb_xSr_{1-x}(NO_3)_2$ (21.3 ppm) and smallest for $Ca_xPb_{1-x}(NO_3)_2$ (18.1 ppm), correlating inversely with cationic radius (Ca^{2+} 1.00 Å, Sr^{2+} 1.18 Å, Ba^{2+} 1.35 Å, Pb^{2+} 1.19 Å) (20).

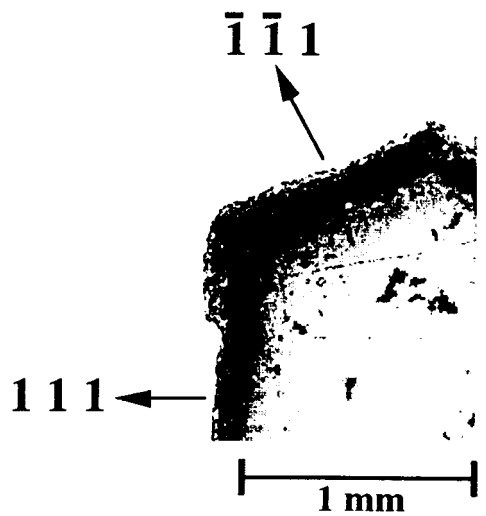

FIG. 8. Backscattered electron micrograph of a $Ba_xPb_{1-x}(NO_3)_2$ crystal. Dark regions indicate Pb^{2+} rich domains.

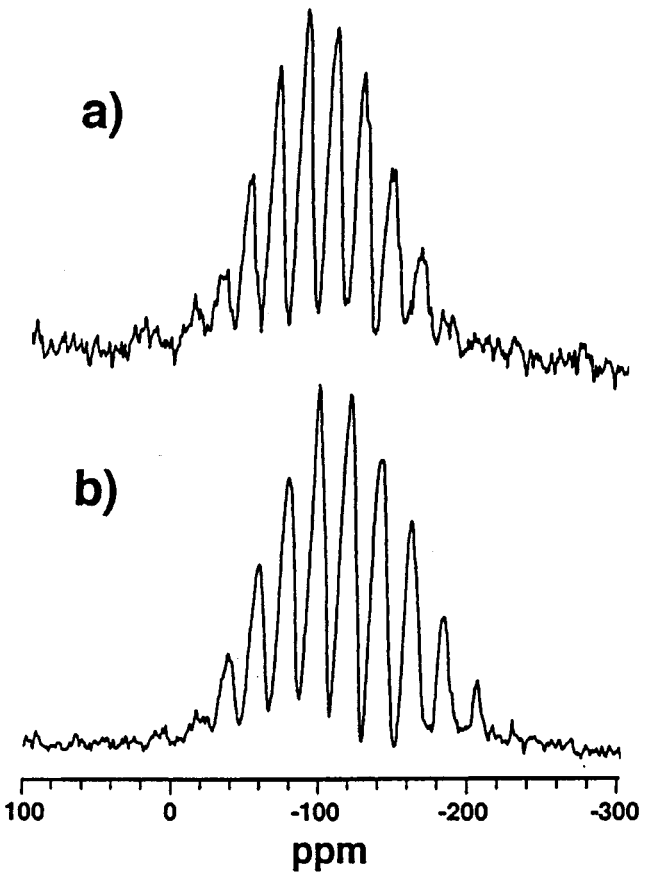

FIG. 9. The ^{207}Pb MAS NMR spectra of precipitated powders of (a) $Ba_{0.42}Pb_{0.58}(NO_3)_2$; (b) $Ba_{0.47}Sr_{0.53}(NO_3)_2$.

Optical Anomalies and Vegard's Rule

The anomalous birefringence of impure crystals of $Pb(NO_3)_2$ was first described by Marbach (21) and later investigated by Klocke (22), Brauns (23), Morel (24), and Wulff (25) in the Nineteenth Century. Despite a multiplicity of opinions regarding the etiology of the phenomenon, no consensus was reached prior to Vegard's powder diffraction experiments which deemphasized the structural importance of optical anomalies. Our X-ray studies presented features that were consistent with the anomalous birefringence but could not serve as proof of the observed optical anisotropy.

Previously, we showed that optically anomalous crystals of $NaCl_xBr_{1-x}O_3$ could be made optically normal by annealing. Concomitant with the changes in optical properties was a randomization of the guest site occupancies (26). Similar experiments could not be carried out with $Ba_xPb_{1-x}(NO_3)_2$. It is known that $Pb(NO_3)_2$, unlike $Ba(NO_3)_2$, tends to include fluid during growth from solution (27). From the comparison of as-grown and annealed crystals in Fig. 10 it is clear that the Pb-rich peaks of the

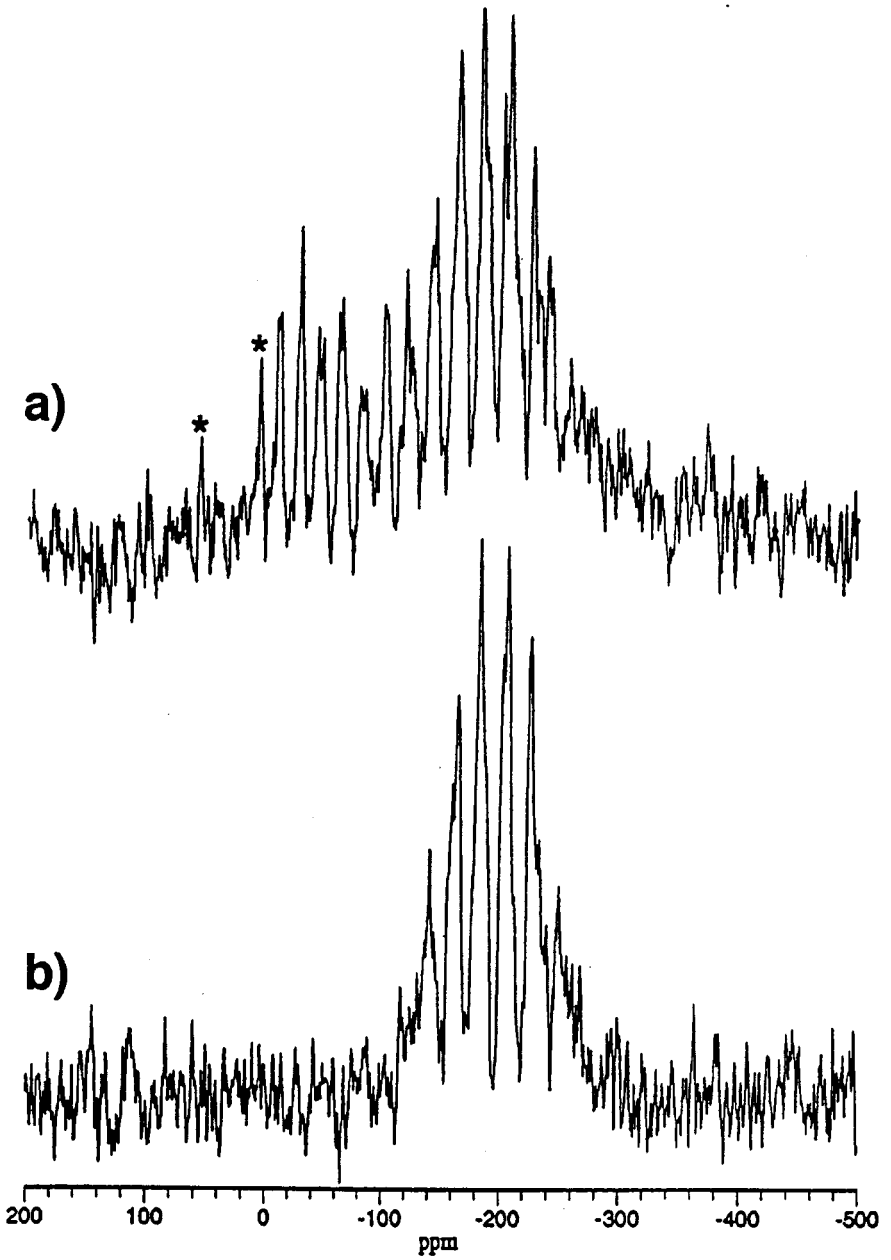

FIG. 10. ^{207}Pb MAS NMR spectra before (a) and after (b) annealing a single powdered crystal of composition $Ba_{0.72}Pb_{0.28}(NO_3)_2$. * marks spinning sidebands.

spectrum disappear upon heating, presumably by conversion to PbO (28).

Tammann first suggested that inhomogeneities could be responsible for the anomalous birefringence (29). Oddly, the anomalous optical properties do not vary systematically, even in crystals such as those in Fig. 8, where the composition clearly changes. Moreover, the optical properties do not readily distinguish between homogeneous and heterogeneous crystals. What is certain is that the crystals originally grown by Vegard that served as the basis for VR must have had bulk heterogeneities, as well as anomalous birefringence. Here, we have used NMR as a test for bulk heterogeneities in the mixed crystals and devised growth conditions which obviate these heterogeneities. In so doing, we have been able to express VR in a novel way by plotting the chemical shifts of the peaks versus the numbers of common ions in the first coordination sphere. A striking linear relationship is once again achieved, a relationship that still fails to signal many of the deviations of as-grown solid solutions of $Ba_xPb_{1-x}(NO_3)_2$ (Fig. 11).

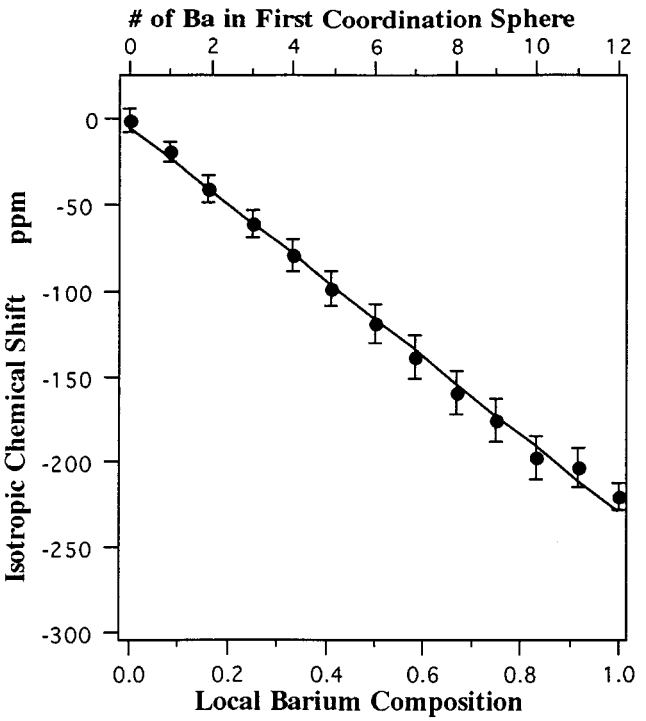

FIG. 11. Number of Ba^{2+} in the first coordination sphere and the local Ba^{2+} composition (% Ba^{2+} = # Ba^{2+} in first coordination sphere/12 on the *x*-axis plotted against the ^{207}Pb isotropic chemical shift for peaks in the MAS NMR spectra of $Ba_xPb_{1-x}(NO_3)_2$ crystals.

ACKNOWLEDGMENTS

We are grateful for financial support from the NSF (CHE-9727372, CHE-9457374) and the donors of the ACS-PRF (30688-AC), as well as the Department of Education for a National Needs Fellowship for J. H. We thank Professor Thomas Bein for access to his powder diffractometer.

REFERENCES

1. L. Vegard and H. Dale, *Z. Krist.* **67,** 148 (1928).
2. R. C. Evans, "An Introduction to Crystal Chemistry," p. 144. Cambridge Univ. Press, Cambridge, 1939. [H. Krebs (P. H. L. Walter, transl.), "Fundamentals of Inorganic Crystal Chemistry," p. 334. McGraw–Hill, London, 1968; B. K. Vainshteiin, V. M. Fridkin, and V. L. Indenborn, "Structure of Crystals," p. 113. Springer-Verlag, Berlin, 1995].
3. V. S. Urusov, *J. Solid State Chem.* **98,** 223 (1992).
4. B. Kahr and J. M. McBride, *Angew. Chem. Int. Ed. Engl.* **31,** 1 (1992).
5. P. Gopalan and B. Kahr, *J. Solid State Chem.* **107,** 563 (1993).
6. M. Fechtelkord and U. Bismayer, *Solid State NMR* **11,** 231 (1998).
7. F. Fayon, I. Farnan, C. Bessada, J. Coutures, D. Massiot, and J. P. Coutures, *J. Am. Chem. Soc.* **119,** 6837 (1997).
8. C. N. R. Rao, K. Vidyasagar, and J. Gopalakrishnan, *J. Solid State Chem.* **58,** 29 (1985).
9. R. Adams, Ph.D. dissertation, Purdue University, 1995.
10. H. Nowotny and G. Heger, *Acta Cryst. Sect. C* **39,** 952 (1983).
11. H. Nowotny and G. Heger, *Acta Cryst. Sect. C* **42,** 133 (1986).
12. L. H. Piette and H. E. Weaver, *J. Chem. Phys.* **28,** 735 (1958).
13. A. Nolle, *Naturforsch. A* **32,** 964 (1977).
14. D. R. Lide (Ed.), "CRC Handbook of Chemistry and Physics," 71st ed. CRC, Boca Raton, FL, 1990.
15. G. Pólya, *Comptes Rendus* **201,** 1167 (1935). [G. Pólya, *Comptes Rendus* **93,** 415 (1936); G. Pólya, *Acta. Math.* **68,** 145, (1937); D. H. Rouvray, *Chem. Soc. Rev.* **3,** 355 (1974)].
16. R. A. Santos, P. Tang, W.-J. Chien, D. Kwan, and G. S. Harbison, *J. Phys. Chem.* **94,** 2717 (1990).
17. P. J. Barrie, C. J. Groombridge, J. Mason, and E. A. Moore, *Chem. Phys. Lett.* **219,** 491 (1994).
18. J. Lefebvre, R. Currant, R. L. Fouret, and M. More, *J. Phys. C* **13,** 4449 (1980).
19. A. Tsuchiyama, M. Kitamura, and I. Sunagawa, *J. Cryst. Growth* **55,** 510 (1981).
20. R. D. Shannon, *Acta Cryst. A* **32,** 751 (1976).
21. H. Marbach, *Ann. Phys. Chem.* **170,** 412 (1855).
22. F. Klocke, *Neues Jahrb. Mineral Geol. Paläontol.* **1,** 53, 158 (1880).
23. R. Brauns, *Neues Jahrb. Mineral Geol. Paläontol.* **II,** 102 (1883); **I,** 138 (1887). [R. Brauns, "Die optischen Anomalien der Krystalle," p. 208. Hirzel, Leipzig, 1891]
24. J. Morel, *Bull. Miner. Soc. Fr.* **10,** 318 (1887); **11,** 230 (1888).
25. G. Wulff, *Z. Krist.* **31,** 511 (1899).
26. P. Gopalan, M. L. Peterson, G. Crundwell, and B. Kahr, *J. Am. Chem. Soc.* **115,** 3366 (1993). [G. Crundwell, P. Gopalan, A. Bakulin, M. L. Peterson, and B. Kahr, *Acta Cryst. Sect. B* **53,** 189 (1997)].
27. I. Sunagawa, K. Maiwa, and K. Tsukamoto, *J. Cryst. Growth* **82,** 611 (1987). [I. Sunagawa, K. Omuma, and K. Tsukamoto, *J. Cryst. Growth* **98,** 384 (1989); I. Sunagawa, K. Maiwa, K. Tsukamoto, C. Ge, and N. Ming, *J. Cryst. Growth* **98,** 590 (1989)].
28. D. A. Bass and J. A. Holcombe, *Anal. Chem.* **64,** 2743 (1992).
29. G. Tammann and W. Krings, *Z. Anorg. All. Chem.* **130,** 229 (1923).